

Deep Anatomical Federated Network (Dafne): an open client/server framework for the continuous collaborative improvement of deep-learning-based medical image segmentation

Francesco Santini^{1,2,3*}, Jakob Wasserthal², Abramo Agosti⁴, Xenia Deligianni^{1,2}, Kevin R. Keene⁵, Hermien E. Kan⁶, Stefan Sommer^{7,8,9}, Christoph Stuprich¹⁰, Fengdan Wang¹¹, Claudia Weidensteiner^{1,3}, Giulia Manco¹², Matteo Paoletti¹², Valentina Mazzoli¹³, Arjun Desai^{13,14}, and Anna Pichiecchio^{12,15}

1. Basel Muscle MRI, Department of Biomedical Engineering, University of Basel, Basel, Switzerland
2. Department of Radiology, University Hospital Basel, Basel, Switzerland
3. Division of Radiological Physics, Department of Radiology, University Hospital Basel, Basel, Switzerland
4. Department of Mathematics, University of Pavia, Pavia, Italy
5. Department of Neurology, Leiden University Medical Center, Leiden, The Netherlands
6. C.J. Gorter MRI Center, Department of Radiology, Leiden University Medical Center, Leiden, The Netherlands
7. Siemens Healthineers International AG, Zurich, Switzerland
8. Swiss Center for Musculoskeletal Imaging (SCMI), Balgrist Campus, Zurich, Switzerland
9. Advanced Clinical Imaging Technology (ACIT), Siemens Healthineers International AG, Lausanne, Switzerland
10. University Hospital Erlangen, Erlangen, Germany
11. Peking Union Medical College Hospital, Beijing, China
12. Advanced imaging and radiomics center, Neuroradiology Department, IRCCS Mondino Foundation, Pavia, Pavia, Italy
13. Department of Radiology, Stanford University, Stanford, CA, USA
14. Department of Electrical Engineering, Stanford University, Stanford CA, USA
15. Department of Brain and Behavioural Sciences, University of Pavia, Pavia, Italy

* Correspondence to:

Francesco Santini
Department of Radiology
University Hospital Basel,
Petersgraben 4
4031 Basel
Switzerland

Abstract

Semantic segmentation is a crucial step to extract quantitative information from medical (and, specifically, radiological) images to aid the diagnostic process, clinical follow-up, and to generate biomarkers for clinical research. In recent years, machine learning algorithms have become the primary tool for this task. However, its real-world performance is heavily reliant on the comprehensiveness of training data. Dafne is the first decentralized, collaborative solution that implements continuously evolving deep learning models exploiting the collective knowledge of the users of the system. In the Dafne workflow, the result of each automated segmentation is refined by the user through an integrated interface, so that the new information is used to continuously expand the training pool via federated incremental learning. The models deployed through Dafne are able to improve their performance over time and to generalize to data types not seen in the training sets, thus becoming a viable and practical solution for real-life medical segmentation tasks.

Main

Introduction

Semantic segmentation of medical (and, specifically, radiological) images is a challenging yet important step towards the automation of both research and clinical workflows, either because it supports the radiologists in highlighting the presence of lesions, or because it is a necessary step in extracting quantitative biomarkers, such as organ size and volume, and average tissue properties over anatomical regions.

The current highest-performing methods for automated image segmentations are based on deep neural networks, typically trained on manually labeled data ¹⁻³. One of the key factors that contribute to the success of these algorithms is the availability of large and diverse training datasets. A high volume of training data allows the algorithm to learn a wide range of features and patterns, which enables it to generalize better to new and unseen examples ⁴. High variability in the training data, on the other hand, helps the algorithm to learn robust and invariant representations, which allows it to perform well in various conditions and environments ⁵.

This is particularly relevant in Magnetic Resonance Imaging (MRI), where there is a large potential variability in the acquisition protocols of the same organ, which results in different contrasts and resolutions, and especially in the imaging of deformable organs such as the skeletal muscles.

In the specific field of muscle MRI, which is useful in the diagnosis and follow-up of neuromuscular diseases and other neuromuscular pathologies, the collection of a representative amount of training data is particularly difficult as many of these are rare. Moreover, clear tissue boundaries are often lacking, and they are additionally blurred in the presence of fat replacement and infiltration. For these reasons, manual segmentation is still the gold standard ⁶, and although some automated methods are present in the literature ⁷⁻¹⁰, they are trained and validated on a limited number of cases, and often limited to healthy muscles or to a subset of pathologic appearances.

A now common solution to the difficulty of collecting all the necessary training data in a single institution is the use of federated learning ¹¹, or, in its decentralized form, swarm learning ^{12,13}, where the same model is trained at different locations on local data, and the model parameters are then aggregated and redistributed multiple times for various training cycles, with the goal of obtaining a final, stable model. This approach is highly appealing in healthcare, as it largely overcomes the legal and practical hurdles of sharing patient data ¹⁴. Indeed, a number of existing studies have been focused on lesion detection and/or classification ¹⁵⁻²⁴ finding similar performance between centralized and federated learning ²⁵.

Despite the very active research area, clinical translation of fully automated segmentation pipelines is challenging, as regulatory bodies require assumption of responsibility for healthcare decisions, and accuracy thus needs to be ensured in a wide range of contexts outside the initial development and testing conditions. A much more practical solution is therefore to integrate segmentation models in image visualization interfaces, giving the user the final control over the accuracy of the segmentation ^{26,27}. By using this approach, the segmentation does not need to be accurate and reliable every time, because an expert human operator will always have the final responsibility over the results. The necessary presence of a human verifier represents the ideal case for the implementation of continuous training of the deep learning models, which can continue over the whole lifetime of the model, learning and adapting to new data.

For this reason, we are proposing a paradigm shift in medical image segmentation, moving away from the traditional training-validation-deployment model, where the model is optimized for a specific data type, towards a more practical workflow that exploits the human knowledge and the collaborative effort of the community to continuously refine the segmentation models. With this approach, we can leverage large amounts of data covering a wide spectrum of real-world applications in a way that is 1) convenient for the end user, 2) privacy-preserving, 3) resource-sparing, and 4) free of medical responsibility because the end

result is always checked by a human operator.

In this paper, we are presenting an open-source, multiplatform client/server software system that integrates deep-learning segmentation models with an advanced user interface for computer-assisted manual segmentation tasks. While the interface already implements a number of advanced features that make it a potentially useful tool on its own, the strength of the system lies in the seamless coupling of this interface with an incremental upgrade of the model performed on the client's side. All the local upgrades are then transmitted to the central server which updates and redistributes the refined model to all users.

This system was designed with the following fundamental principles in mind, reflecting the features stated above:

1. The program has an intuitive user interface with advanced manual editing features (user convenience).
2. Data are only handled by the client and never transmitted (privacy preservation).
3. Incremental learning is performed on the client's side (resource sparing).
4. The automated segmentation is always checked and refined by the operator (waiver of medical responsibility).

The system was named Dafne (an acronym for Deep Anatomical Federated Network), and currently offers two models that are specialized in the segmentation of the skeletal muscles of the leg and thigh in health and disease. We tested Dafne both in a controlled study of locally collected data (38 clinical MRI datasets) and in a retrospective analysis of the system performance in terms of native segmentation quality during the distributed usage over a period of 18 months, which amounted to 639 segmented datasets segmented by 36 independent users.

We demonstrate that by following these principles, Dafne is a practical and effective tool that can be used by medical professionals in clinical research that is capable of autonomously improving its performance over time.

Results

Dafne was first distributed to users in April 2021 in a testing phase, and a significant expansion of the user base (from 9 initial test users to 25) started in the summer of 2021. The user base expanded to 36 active users by the end of the considered period (December 2022). The client side of Dafne is a feature-rich image viewer with computer-aided manual segmentation capabilities, which interacts with a server that provides continuously updated neural network models for image segmentation, encapsulated in serialized executable objects that are dynamically integrated into the client at runtime. These objects are self-contained and are able to perform the necessary pre- and post-processing steps in addition to the network prediction, for optimal flexibility.

Over the course of Dafne's lifetime, we collected real-world usage data and performed testing under controlled conditions. The data collected (anonymized for privacy reasons), together with the code to perform the analysis presented in the following paragraphs and to generate the figures, are available under a CC-BY license at ²⁸.

Workflow from the user perspective

Dafne implements a client/server architecture. The server, including a website containing the documentation, is hosted on a Google Cloud Virtual Machine (Google LLC, Mountain View, CA, USA) at the web address <https://dafne.network/>. The role of the server is to provide the available segmentation models to the client and receive updated versions from the users and integrate them into the central model (see the Method section for details).

The user downloads the Dafne client either in packaged form (available for Microsoft Windows, Apple MacOS, and GNU/Linux) or in source form from the Github repository page or the Python Package Index (PyPI). A personal API key, currently distributed for free through a request form on the website, enables

communication between the client and the server.
Once the connection is established, the client is ready for usage.

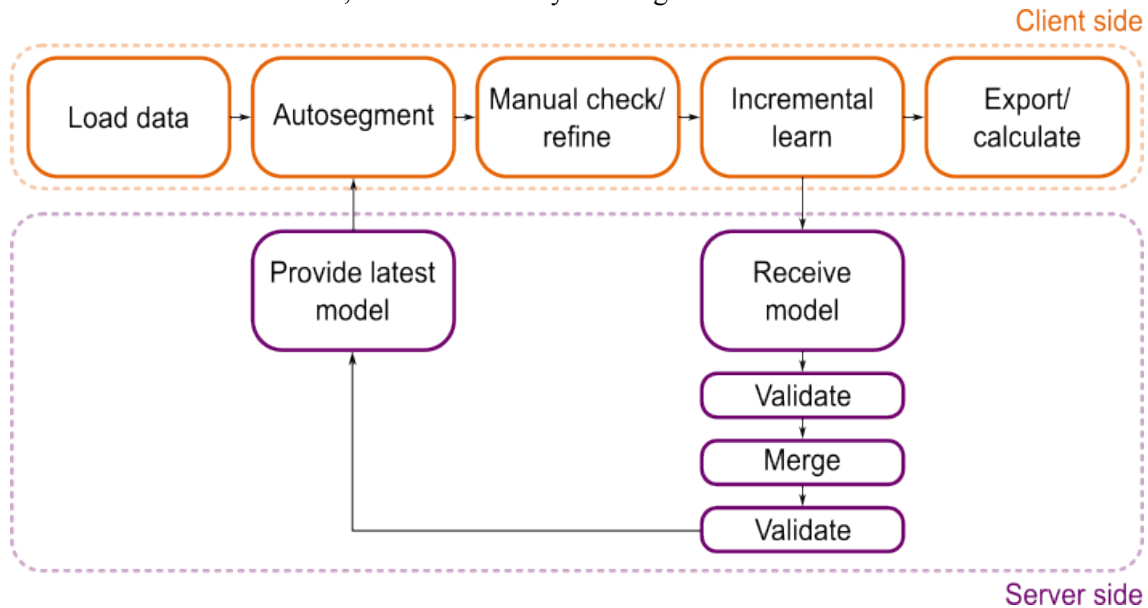


Figure 1: Dafne workflow. The top flow happens on the client’s side, with user interaction in the manual refinement step. When the user exports the segmented masks, or calculates the voxel statistics from within the software, an incremental learning step over the used model is triggered. The bottom flow happens automatically on the server once a refined model is received.

The typical Dafne workflow is shown in Fig. 1. The user loads the data (a variety of common medical imaging formats, including classic and enhanced DICOM²⁹ and NIfTI³⁰, is supported), and selects one model to be used for the segmentation. Two models are provided: the “leg” model, segmenting 6 muscles of the human lower leg, and the “thigh” model, segmenting 12 muscles of the thigh. Both models work on single axial slices, with the option in the client of reformatting the datasets if they are originally in a different orientation. There are also variants of each model that can be applied to images of both limbs or of a single (left or right) limb. The variants rely on the same machine learning model with different pre- and postprocessing steps.

Once the data are loaded, the user is shown the main interface (Fig. 2). The dataset is shown slice-by-slice (a common modality for many medical image viewers), which the user can scroll through and modify the brightness and contrast. By using the “Autosegment” button, the latest model for the selected body region is downloaded from the server and applied to one or more slices. After segmentation, various editing tools are used for the refinement of the labeled areas. Variable-brush-size manual area painting and erasing is the primary tool used (“mask” modality); however, a “contour” modality enables the editing of the contours of the labeled areas by modifying the handles of an interpolating spline curve, which is useful in case of the definition of whole new areas. Switching between the contour and mask modalities can be performed seamlessly.

Depending on the edit modality, various editing tools are available, including nonrigid-registration-based area propagation and interpolation, image-gradient-based contour snapping, common mask operations (area opening and closing, thresholding), etc. A full description of the features is available in the user documentation³¹.

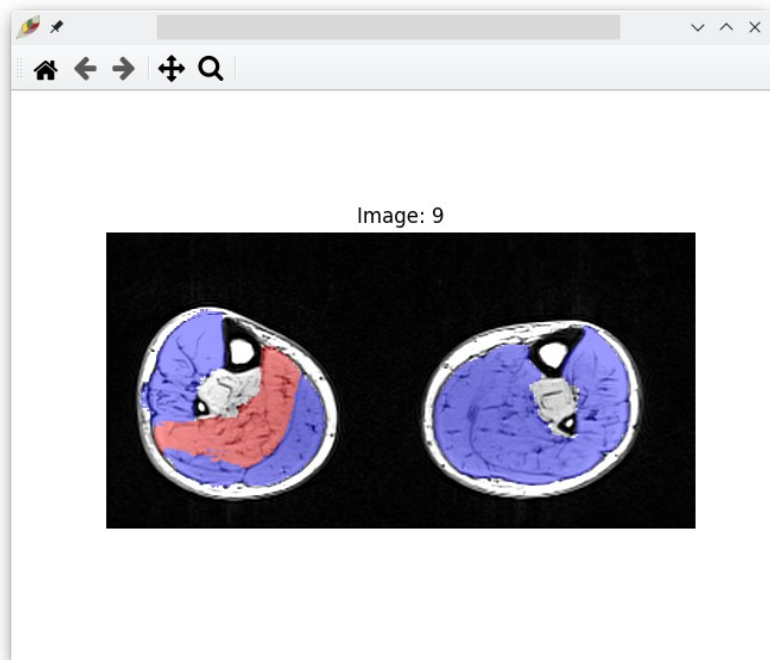
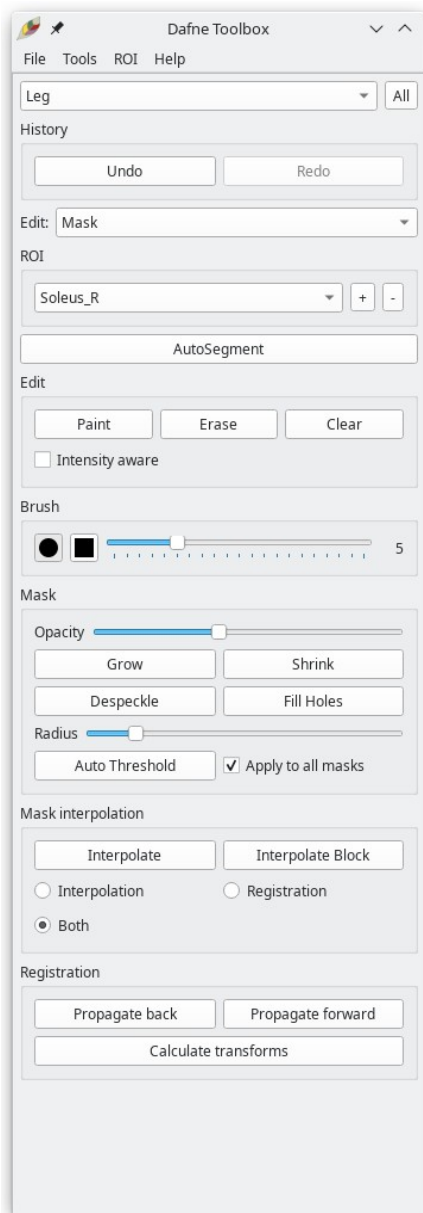


Figure 2: Screenshot of the Dafne user interface. Dafne is currently in “mask” edit mode and the corresponding tools are shown on the toolbox on the left. The active region of interest (in this case the right Soleus muscle) is overlaid in red in the image window. The inactive regions are overlaid in blue.

Once the user has checked and refined the automatic segmentation, the masks can either be exported for further processing, voxel statistics (intensity over each ROI, number of voxels, volume, etc.) can be directly calculated, and radiomics feature extraction (based on pyradiomics³²) can be performed. During this last step, if the number of segmented slices is sufficient (at least 5), model refinement is triggered, consisting of 5 epochs of incremental learning, as described in¹⁰.

The model is then automatically sent back to the server, where it first gets validated on internal data, and then, if successful, merged with the previous version of the model and made available for the next usage.

In order to provide a certain usefulness to the users from the beginning, the initially provided models were already pretrained on a limited set of proton-density-weighted MRI data¹⁰.

In Fig. 3, we show how the “leg” model visually improved over the course of collaborative usage, by showing the output of the automatic segmentation for two model snapshots: the initial pretrained one, and one taken in November 2022. The proton-density contrast was acquired with a similar protocol as the dataset on which the initial models were pretrained; the T1 contrast is instead a new contrast that the initial

pretrained model was never exposed to. A visually clear improvement can be observed for both image contrasts.

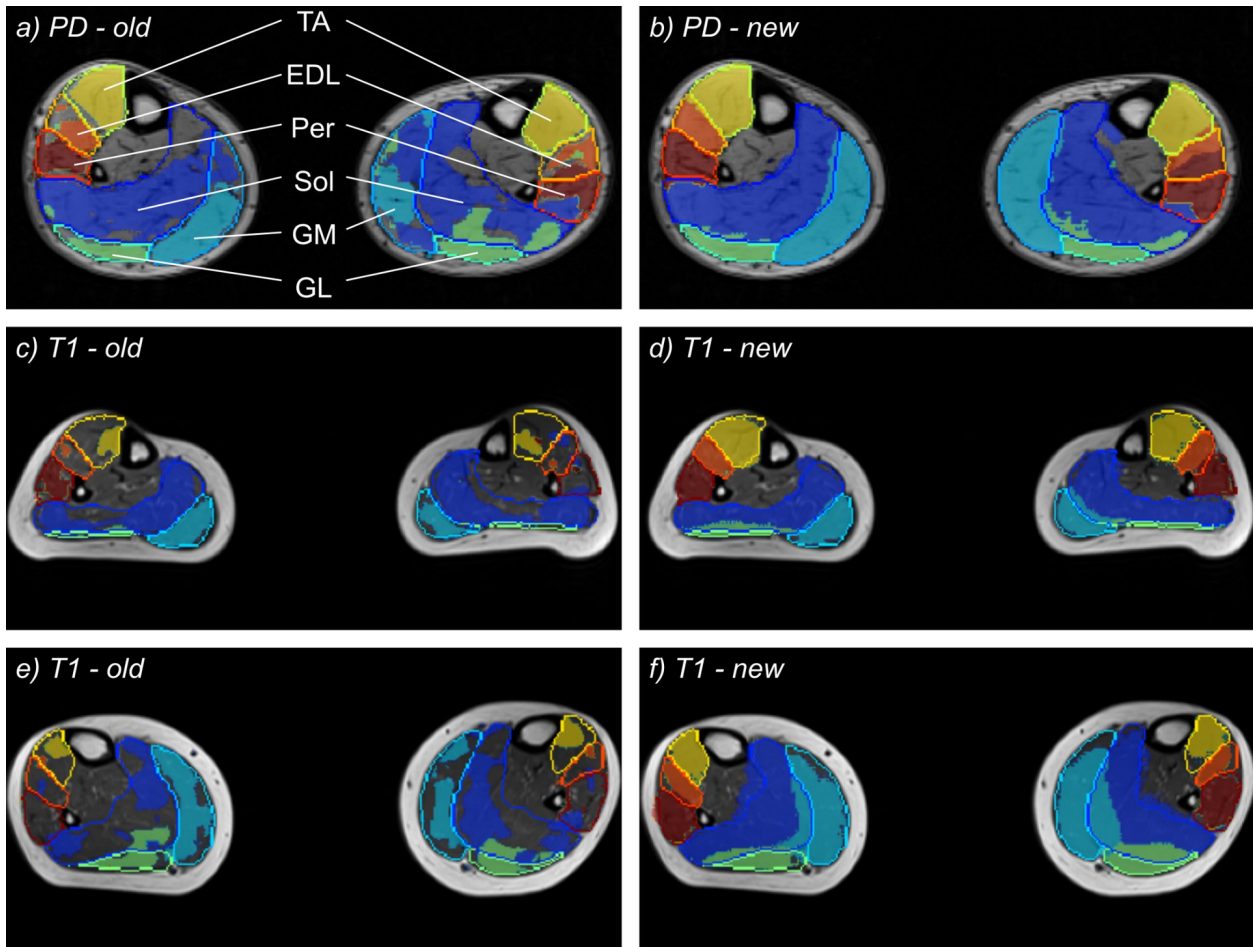


Figure 3: Segmentation example at two different time points and three different datasets. Panels *a* and *b* show a proton-density weighted dataset (the same contrast used in the pretraining) segmented with the initial pretrained model (*a*) and with the most current model (*b*). Panels *c* to *f* show T1-weighted datasets (a contrast not included in the pretraining) segmented with the initial model (*c* and *e*) and with the current model (*d* and *f*). The outlines around the muscles show a ground-truth manual segmentation, and the semitransparent areas show the result of the automatic segmentation. On the first panel, the labeling of the muscles is shown (TA: Tibialis Anterior; EDL: Extensor Digitorum Longus; Per: Peroneus; Sol: Soleus; GM: Gastrocnemius Medialis; GL: Gastrocnemius Lateralis). In the last panel, an overestimation of the gastrocnemii by the automatic algorithm is shown. This case is especially difficult because muscle boundaries are not clearly visible in the image.

Images available under CC-BY at Ref. 28.

Learning new image contrasts under controlled conditions

We systematically tested the performance of the proposed approach with a retrospective analysis of anonymized clinically collected data performed under a waiver of the requirement for specific informed consent by the local ethical committee. It was performed by analyzing 38 T1-weighted datasets of patients with suspected myositis who received a routine MR examination which included the lower leg.

The 38 datasets were split into two groups, group A containing 25 datasets, and group B containing the remaining 13. Each group was randomly split between two independent annotators, working on different workstations, to mimic the real-world situation of distributed usage.

At least 5 slices in the leg region of each dataset in group A were segmented by the two annotators using the Dafne standard workflow. This means that the datasets in group A were progressively included in the

training for the later datasets. The average Dice Similarity Coefficients (DSCs) ³³ of all the segmented muscles were used as a quality metric to evaluate the quality of the model. It was calculated for each model and each dataset produced during the segmentation of group A, between the automatic and the manually refined segmentation. Considering the DSC at time 0 (the time of the model before the group A segmentation) as the baseline, it can be observed that the average DSC over all the datasets tended to increase (Fig. 4a). By fitting a linear mixed effects model with random slope (dependent on the dataset) to this trend, we observed a significant ($p < 0.001$) increase by 0.009 ± 0.001 points (95% confidence interval 0.006-0.012) per learning step on the group A datasets.

After the segmentation of group A, the same annotators used the Dafne workflow to similarly segment the datasets of group B. However, the model updates generated by group B were excluded from subsequent evaluation. This division ensured that the evaluated models were never trained on any data belonging to group B.

A similar average DSC increase can be observed in group B, on the models refined on the datasets of group A (Fig. 4b). The linear model also revealed a significant increase ($p < 0.001$) with a linear coefficient of 0.007 ± 0.002 points (95% confidence interval 0.003-0.011) per learning step, thus demonstrating that the model incrementally trained on group A successfully generalized to the segmentation of group B.

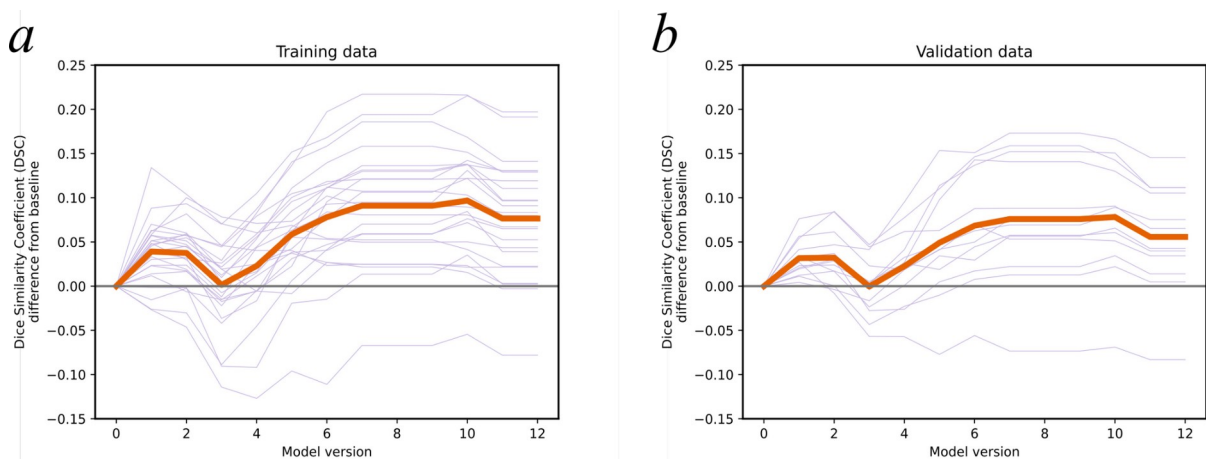


Figure 4: Evolution of the Dice Similarity Coefficients over the model versions produced by the local evaluation. Panel *a* reports the results for the data used for the training (group A in the text), whereas panel *b* reports the results of the data used for validation (group B). The thin gray lines correspond to each dataset, and the thick orange line is the average DSC across all datasets. Plots available under CC-BY at Ref. 28.

Overall performance in real-world conditions

User data statistics in the form of average DSC across all regions of interest and all slices were automatically sent by the client to the server and recorded every time a user finished the segmentation of a dataset. The users were not instructed on a particular segmentation style (e.g. how much margin to leave between adjacent muscles), nor were they restricted to the type of protocol, contrast, or pathology that they could import into the system, as the hypothesis was that the model could generalize to a wide range of inputs and that it would converge towards a consensus segmentation style. To avoid data regulatory concerns, specific patient or pathology data were not collected from the sites.

The user statistics were observed over a period spanning from July 1st, 2021, to December 31st, 2022, and consisted of the collection of averaged DSC for every segmented dataset. The log file also showed how many unique users utilized the system.

Over the considered period, Dafne reached 36 active users, and they collectively segmented 662 datasets. Of these, 639 were considered valid data points, excluding the points that suggested irregular user behavior,

namely perfect dice scores (≥ 0.99 , indicating that no refinement was performed) and dice scores very close to zero (< 0.1 , possibly indicating that a wrong segmentation task was performed). 23 data points (3.5%) were excluded according to these criteria.

The “thigh” model was used on 123 datasets, with a median DSC of 0.88 (interquartile range 0.82 – 0.91). The “leg” model was used on 516 datasets, with a median DSC of 0.82 (interquartile range 0.71 – 0.88).

Analyzing the model evolution over time (Fig. 5), it can be observed that after user growth, the average DSC of the system declined, both for the leg and thigh datasets, which was the expected behavior, compatible with the introduction of different contrasts and protocols previously unknown to the original models; however, the DSC recovered over the course of the usage and reached consistently high values after user number stabilization.

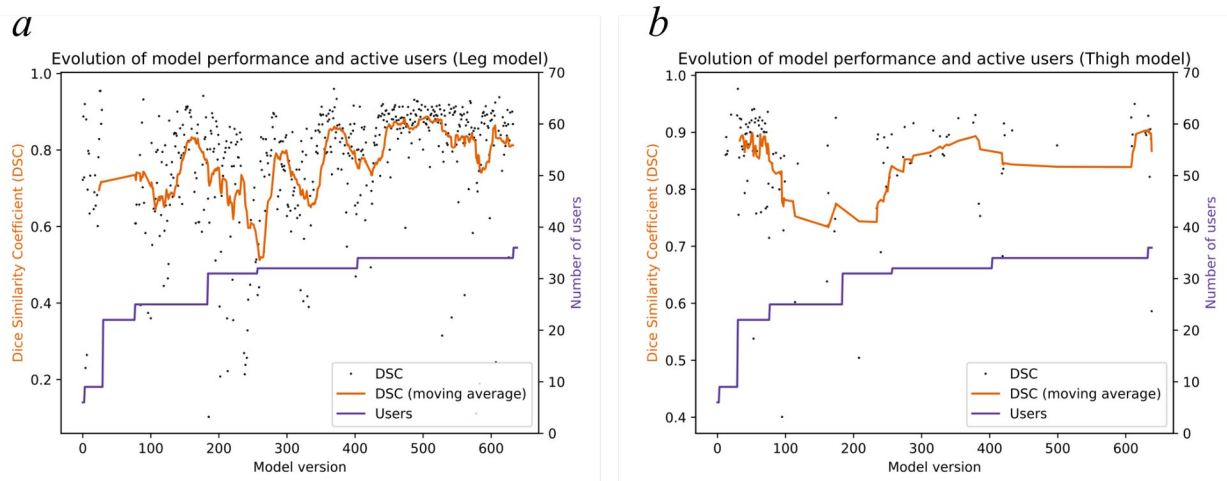


Figure 5: Evolution of model performance for both the leg (a) and thigh (b) models over time, as reported by the client, together with number of active users (in purple). For both models, an initial decline after user expansion can be observed, which then recovers after stabilization of user numbers. Plots available under CC-BY at Ref. 28.

Discussion

We presented Dafne, a fully open client/server software package and development framework for the segmentation of medical images which allows lifelong federated learning and is a solution to the problem of low availability of data, especially when rare conditions are investigated and direct data sharing is not feasible or desirable for legal or practical reasons.

We demonstrated that the system is able to adapt to new image contrasts (through a controlled study where T1 contrast was used, as opposed to the proton-density contrast of the initial training) and that its performance is able to adapt to the requirements of a growing set of users, by achieving overall improved quality over time.

Specifically, the “leg” segmentation model showed an overall increase in its average performance in comparison with the early results; the “thigh” model reported high-performance values in its early stages, when the user pool was still small, followed by a decline and a subsequent recovery. This behavior is expected and is an indication of the initial low adaptation of the model to new image protocols and contrasts, which it incorporated in the later stages.

One key component of the task was developing a user-friendly interface for loading and manually segmenting (or refining the existing segmentation) medical datasets in multiple formats. This allowed for a natural workflow for medical professionals, who could proficiently exploit the system and have complete control over the end results. The feasibility and convenience of this proposed workflow was already demonstrated in a previous study by Wang et al ³⁴.

The health conditions that require segmentation of the skeletal muscles from MR images for diagnostic

purposes are for the most part rare, and are primarily investigated by a range of non-standardized qualitative MR imaging protocols³⁵. Such protocols, such as T1-weighted imaging or fat-suppressed T2-weighted imaging, are segmented primarily to extract volumetric information of the muscles of interest for the evaluation of muscle wasting, and they can be acquired with vastly different resolutions and protocol parameters, affecting the relative brightness of the various tissue compartments. Similarly, even the quantitative MR measurements used in clinical research (quantitative fat fraction and quantitative T2), can be performed by a variety of gradient-echo or spin-echo based protocols, resulting in images that can be noticeably different across sites. Finally, an additional element of variability is given by the deformable, position-dependent geometry of the limbs (as opposed, for example, to the brain). These factors make the training of a sufficiently general model, which could give well-reproducible results across institutions, difficult.

For this reason, our approach challenges the traditional workflow of training-validation-deployment of a model, to substitute it with a continuously adapting one. While this cannot guarantee a stable performance over time, we believe that it can be most useful in real-world circumstances, where human oversight and assumption of responsibility are necessary for a patient care environment. If the user desires consistency in the results for reproducibility, they can choose to disconnect from the Dafne network and use a particular model version for all their subsequent segmentation tasks. Although not currently implemented in the user interface, the retrieval of old models from the server is also possible through the network application programming interface (API).

The goal of the system is currently focused on the segmentation of muscle anatomy from MR images. As explained above, the complex nature of the task makes it an ideal test case for this kind of approach. However, the application of this system is potentially much more general than this specific application. New models can be easily programmed by following the object interface specification, and immediately deployed through the Dafne infrastructure.

Another advantage of this system is the incremental learning that is performed on the client's side and not on the server. As the training is only performed on a single dataset at a time for a small number of epochs, this poses little penalty to the user, who can perform it on any workstation, even without the usage of a Graphical Processing Unit (GPU). This is a marked distinction from conventional federated learning approaches¹⁵⁻²⁴, which require the training of the model on all the data available at a site, and thus usually require dedicated computing time. At the same time, the same advantage as with federated learning holds for the server, which in our case is a simple CPU-only virtual machine hosted on Google Cloud. The only computationally expensive job on the server is the application of the model on the validation data stored, which is much less intensive than model training.

In the current implementation, Dafne users all contribute to the same model. This is a desired feature because it is necessary to expose the model to the largest variability of input data (in terms of contrasts, data quality, and image characteristics) in order to generalize its applicability. However, different users potentially follow different segmentation guidelines, which would necessarily reduce the stability of the performance of the model, as it will continuously adapt towards the most "popular" segmentation style, a typical characteristic of lifelong learning. This problem can be addressed by implementing selective learning of the different parts of the model, for example by only updating the "encoder" part of the global model (extracting the contrast-related features¹), and keeping a local version of the "decoder" side which deals with the labeling. However, this would create personalized models for each user, which would decrease the reproducibility and standardization of the system. This splitting of the model updates could nevertheless allow for more powerful models, which could use the same encoder structure and weights, but produce different labeling (e.g. to segment fatty tissue or muscle groups instead of single muscles).

In conclusion, Dafne's approach, which substitutes the traditional train-validate-deploy model of machine-learning-based medical image segmentation solution with a lifelong learning approach enabled by human supervision, is demonstrably capable of improving and generalizing on new data provided by the users and can be a viable and practical solution in real-world clinical situations.

Acknowledgment

The Authors would like to acknowledge all the active users of Dafne, and their precious feedback. This work has been partly supported by the Swiss National Science Foundation (SNF) Spark grant number CRSK-3_196515. Part of the authors of this paper are members of the EURO-NMD European Reference Network.

Methods

Client/server implementation

Both the client and the server components of Dafne are programmed in Python and are available as Free and Open Source Software on Github (<https://github.com/dafne-imaging>). The client is installable through the Python Package Index (PyPI) and prepackaged binaries are provided for Microsoft Windows, GNU/Linux, and Apple MacOS.

The Dafne client is a fully-fledged application for the two-dimensional visualization and computer-assisted segmentation of medical images whose interface is based on the PyQt5 (Riverbank Computing Limited, Dorchester, UK) and matplotlib³⁶ graphics libraries with optimized visualization tweaks (e.g. multithreaded operation and blitting³⁷).

Nonrigid registration for the propagation of ROIs across slices is provided by the SimpleElastix³⁸ library, and additional image processing procedures are implemented based on scikit-image³⁹, SciPy⁴⁰, and SimpleITK²⁶. Data I/O is derived from DOSMA⁴¹.

ROI conversion between mask and contour is performed through connectivity filling of the contour (in the contour-to-mask conversion)⁴², or through a custom iterative optimization of the spline until subvoxel accuracy of the contour rendering is achieved (in the mask-to-contour conversion).

The server component is also programmed in Python and currently resides on a cloud-hosted virtual machine (Google Cloud, Google Inc, Mountain View, CA, USA). It is encapsulated in a docker⁴³ image and leverages the FastAPI⁴⁴ library for communication with the client. The core functionality of the server is to provide the most recent model to the client and to receive the updated models after incremental learning on the client's side. No model training is performed on the server's side; instead, every received model is validated against an internal library of manually segmented validation data, by performing a segmentation of the data with the new model and calculating the Dice Similarity Coefficient (DSC)³³ with the stored "gold standard" manually segmented masks. This validation is necessary to exclude models that would unacceptably decrease the model's performance.

The validation is performed once the model is received and, if successful (i.e. the DSC is higher than a predefined threshold), the new model is merged with the existing version.

This merging operation is a simple linear combination of the weights of the old model and of the new model, and it is an operation that is implemented by the model object itself, and it is therefore agnostic to the underlying implementation for optimal generalizability. The weights of the linear combination are defined in a server configuration file and are currently set to 0.5 (i.e. the merged model is an exact average of the weights of the preexisting model and the newly uploaded model).

The merged model is validated again, and, if successful, it replaces the current model as the most recent one which will be served to any client at the next request.

Deep learning models and algorithms

The deep learning model implementation is designed to be generic and extensible through a plugin-like architecture. The most low-level way of exchanging information about a neural network model is to communicate the weights of the neuronal connections forming the model. In our implementation, the models are represented by files that contain a serialized (using the dill python package⁴⁵) representation of a Python object, implementing the functionality of a segmentation model in the most generic way possible. In

practice, the object not only contains the weights of the model, but also contains the functions that perform the initialization of the model, the pre- and postprocessing of the data, the incremental learning, and the averaging of the model weights with another model. All these functions are serialized together with the model weights and used for transmission between the client and the server. If the source code is accessible at runtime, a text version of the function is serialized for best compatibility with different python versions, otherwise the compiled bytecode is included in the serialized object. This approach allows the implementation of virtually arbitrary segmentation algorithms and is potentially agnostic to the underlying machine learning framework.

Two models are currently provided by the Dafne server, and they currently share the same basic implementation. They are able to segment 12 muscles of the thigh (vastus lateralis, medialis, and intermedius, rectus femoris, sartorius, gracilis, adductor magnus and longus, semimembranosus, semitendinosus, and the long and short heads of the biceps femori) and 6 muscles of the lower legs (gastrocnemius lateralis and medialis, soleus, extensor digitorum longus, peroneus, and tibialis anterior), respectively.

They are based on the previous work by Agosti et al ¹⁰, where customized versions of the VNet ³ and ResNet ⁴⁶ architectures for deep convolutional networks were used. These networks employed a contracting topology for classification tasks and extracting deep features from increasingly compressed levels of resolution. An expanding topology was employed for resolution decompression and performing the segmentation task. The models were pretrained on 44 datasets in order to provide an initial working implementation for the users and to avoid catastrophic forgetting during subsequent incremental learning steps ⁴⁷. These 44 datasets were axial proton-density-weighted gradient echo acquisitions of the leg and thigh, with a resolution of 1.04x1.04x5.0mm³, with the field of view containing both the right and left limbs. The network architecture, the training data and the training procedure are described in detail in Agosti et al ¹⁰, and implemented using the Tensorflow ⁴⁸ and Keras ⁴⁹ libraries. However, the models were adapted with the goal of being applicable to a wider range of acquisition protocols. While the original implementation was using a single convolutional network for the bilateral segmentation of both limbs, in the current implementation the models were modified to only segment one single limb, thus being able to accommodate multiple choices of fields of view. A preprocessing step was included in the model code to appropriately split and mirror the input images where necessary. Similarly, the input images are preprocessed to adapt the size and resolution to the original training data. By removing the dependency on the resolution and image size, the main source of variability in the data introduced by the widespread release of the model to multiple users is the image contrast, which can vary significantly in MR acquisitions. Incremental learning is performed on each used model every time a segmentation on a minimum of five slices is performed by a user. The incremental learning consists of five epochs of training of the model on the refined images by using a batch size of 5 and an Adam optimizer ⁵⁰, employing a class-balanced weighted cross-entropy loss function, where the weights are calculated in a preprocessing step and compensate the different frequency of pixels for each segmentation class, while focalizing the attention of the network between neighboring muscles, as in ¹⁰.

Performance evaluation

The main performance indicator used to evaluate Dafne is the average Dice Similarity Coefficient (DSC). It was calculated for each ROI and for each slice in the segmented dataset with the formula:

$$DSC = \frac{2(ROI_{auto} \cap ROI_{refined})}{ROI_{auto} + ROI_{refined}},$$

where $ROI_{auto} \cap ROI_{refined}$ is the number of common voxels between the automatically segmented ROI and the manually refined one.

The average (global) DSC for the whole was calculated by taking an average of the DSC for each ROI and slice, weighted by the number of voxels of each manually refined ROI.

DSCs were analyzed separately for the leg and thigh datasets.

The local evaluation was a retrospective analysis of anonymized clinically collected data performed under a waiver for the requirement for informed consent provided by the local ethics committee. It was performed by analyzing 38 datasets of patients with suspected myositis who received a routine MR examination which included both lower legs. The acquisition protocol was a 2D axial T1-weighted turbo spin-echo sequence, covering both limbs with a resolution of 1.04x1.04x8.0mm³. Thus, while the resolution was similar to the initial training data, these datasets had a different contrast, to ensure that the performance of the system to generalize to different contrasts was tested.

The statistical evaluation of the DSC trend was performed in Python (Jupyter Notebook) by using a linear mixed effects model (mixedlm class of the statsmodels package ⁵¹).

As the first point is forcibly set to 0 because of the calculation of the relative DSC, the intercept of the model is constrained to 0, thus resulting in the formula:

$$relative_score \sim 0 + model_version + (model_version|dataset).$$

References

1. Badrinarayanan, V., Kendall, A. & Cipolla, R. SegNet: A Deep Convolutional Encoder-Decoder Architecture for Image Segmentation. Preprint at <https://doi.org/10.48550/arXiv.1511.00561> (2016).
2. Ronneberger, O., Fischer, P. & Brox, T. U-Net: Convolutional Networks for Biomedical Image Segmentation. *ArXiv150504597 Cs* (2015).
3. Milletari, F., Navab, N. & Ahmadi, S.-A. V-Net: Fully Convolutional Neural Networks for Volumetric Medical Image Segmentation. *ArXiv160604797 Cs* (2016).
4. Goodfellow, I., Bengio, Y. & Courville, A. *Deep learning*. (The MIT Press, 2016).
5. Krizhevsky, A., Sutskever, I. & Hinton, G. E. ImageNet Classification with Deep Convolutional Neural Networks. in *Advances in Neural Information Processing Systems* vol. 25 (Curran Associates, Inc., 2012).
6. Barnouin, Y. *et al.* Manual segmentation of individual muscles of the quadriceps femoris using MRI: A reappraisal. *J. Magn. Reson. Imaging* **40**, 239–247 (2014).
7. Yao, J., Kovacs, W., Hsieh, N., Liu, C.-Y. & Summers, R. M. Holistic Segmentation of Intermuscular Adipose Tissues on Thigh MRI. in *Medical Image Computing and Computer Assisted Intervention – MICCAI 2017* (eds. Descoteaux, M. *et al.*) vol. 10433 737–745 (Springer International Publishing, 2017).
8. Anwar, S. M. *et al.* Semi-Supervised Deep Learning for Multi-Tissue Segmentation from Multi-Contrast MRI. *J. Signal Process. Syst.* (2020) doi:10.1007/s11265-020-01612-4.
9. Ding, J. *et al.* Deep learning-based thigh muscle segmentation for reproducible fat fraction quantification using fat–water decomposition MRI. *Insights Imaging* **11**, 128 (2020).
10. Agosti, A. *et al.* Deep learning for automatic segmentation of thigh and leg muscles. *Magma N. Y. N* (2021) doi:10.1007/s10334-021-00967-4.
11. McMahan, B., Moore, E., Ramage, D., Hampson, S. & Arcas, B. A. y. Communication-Efficient Learning of Deep Networks from Decentralized Data. in *Proceedings of the 20th International Conference on Artificial Intelligence and Statistics* 1273–1282 (PMLR, 2017).
12. Saldanha, O. L. *et al.* Swarm learning for decentralized artificial intelligence in cancer histopathology. *Nat. Med.* **28**, 1232–1239 (2022).
13. Warnat-Herresthal, S. *et al.* Swarm Learning for decentralized and confidential clinical machine learning. *Nature* **594**, 265–270 (2021).
14. van Panhuis, W. G. *et al.* A systematic review of barriers to data sharing in public health. *BMC Public Health* **14**, 1144 (2014).
15. Ul Alam, M. & Rahmani, R. Federated semi-supervised multi-task learning to detect covid-19 and lungs segmentation marking using chest radiography images and raspberry pi devices: An internet of medical things application. *Sensors* **21**, (2021).
16. Kumar, R. *et al.* Blockchain-Federated-Learning and Deep Learning Models for COVID-19 Detection

- Using CT Imaging. *IEEE Sens. J.* **21**, 16301–16314 (2021).
17. Abdulkareem, M. & Petersen, S. E. The Promise of AI in Detection, Diagnosis, and Epidemiology for Combating COVID-19: Beyond the Hype. *Front. Artif. Intell.* **4**, (2021).
 18. Yang, D. *et al.* Federated semi-supervised learning for COVID region segmentation in chest CT using multi-national data from China, Italy, Japan. *Med. Image Anal.* **70**, (2021).
 19. Sheller, M. J., Reina, G. A., Edwards, B., Martin, J. & Bakas, S. Multi-institutional Deep Learning Modeling Without Sharing Patient Data: A Feasibility Study on Brain Tumor Segmentation. in *Brainlesion: Glioma, Multiple Sclerosis, Stroke and Traumatic Brain Injuries* (eds. Crimi, A. et al.) 92–104 (Springer International Publishing, 2019). doi:10.1007/978-3-030-11723-8_9.
 20. Li, W. *et al.* Privacy-preserving Federated Brain Tumour Segmentation. *ArXiv191000962 Cs* (2019).
 21. Yi, L. *et al.* SU-Net: An Efficient Encoder-Decoder Model of Federated Learning for Brain Tumor Segmentation. *Lect. Notes Comput. Sci. Subser. Lect. Notes Artif. Intell. Lect. Notes Bioinforma.* **12396 LNCS**, 761–773 (2020).
 22. Camajori Tedeschini, B. *et al.* Decentralized Federated Learning for Healthcare Networks: A Case Study on Tumor Segmentation. *IEEE Access* **10**, 8693–8708 (2022).
 23. Shen, C. *et al.* Multi-task Federated Learning for Heterogeneous Pancreas Segmentation. *Lect. Notes Comput. Sci. Subser. Lect. Notes Artif. Intell. Lect. Notes Bioinforma.* **12969 LNCS**, 101–110 (2021).
 24. Roth, H. R. *et al.* Federated Whole Prostate Segmentation in MRI with Personalized Neural Architectures. *Lect. Notes Comput. Sci. Subser. Lect. Notes Artif. Intell. Lect. Notes Bioinforma.* **12903 LNCS**, 357–366 (2021).
 25. Czeizler, E. *et al.* Using federated data sources and Varian Learning Portal framework to train a neural network model for automatic organ segmentation. *Phys. Med.* **72**, 39–45 (2020).
 26. Lowekamp, B. C., Chen, D. T., Ibáñez, L. & Blezek, D. The Design of SimpleITK. *Front. Neuroinformatics* **7**, (2013).
 27. Kikinis, R., Pieper, S. D. & Vosburgh, K. G. 3D Slicer: A Platform for Subject-Specific Image Analysis, Visualization, and Clinical Support. in *Intraoperative Imaging and Image-Guided Therapy* (ed. Jolesz, F. A.) 277–289 (Springer, 2014). doi:10.1007/978-1-4614-7657-3_19.
 28. Francesco Santini. GitHub - dafne-imaging/dafne-evaluation: Evaluation and figure generation for Dafne. <https://github.com/dafne-imaging/dafne-evaluation>.
 29. NEMA PS3 / ISO 12052. *Digital Imaging and Communications in Medicine (DICOM) Standard*. (National Electrical Manufacturers Association).
 30. Cox, R. W. *et al.* A (sort of) new image data format standard: NiFTI-1. in vol. 22 (2004).
 31. Santini, F., Wasserthal, J. & Agosti, A. Dafne - Deep Anatomical Federated Network - Documentation. (2022) doi:10.5281/zenodo.7568156.
 32. van Griethuysen, J. J. M. *et al.* Computational Radiomics System to Decode the Radiographic Phenotype. *Cancer Res.* **77**, e104–e107 (2017).
 33. Dice, L. R. Measures of the Amount of Ecologic Association Between Species. *Ecology* **26**, 297–302 (1945).
 34. Wang, F. *et al.* Assessment of idiopathic inflammatory myopathy using a deep learning method for muscle T2 mapping segmentation. *Eur. Radiol.* (2022) doi:10.1007/s00330-022-09254-9.
 35. Carlier, P. G., Mercuri, E. & Straub, V. Applications of MRI in muscle diseases. *Neuromuscul. Disord. NMD* **22 Suppl 2**, S41 (2012).
 36. Hunter, J. D. Matplotlib: A 2D Graphics Environment. *Comput. Sci. Eng.* **9**, 90–95 (2007).
 37. Sanchez, J. & Canton, M. P. *Software solutions for engineers and scientists*. (CRC Press, 2008).
 38. Marstal, K., Berendsen, F., Staring, M. & Klein, S. SimpleElastix: A User-Friendly, Multi-lingual Library for Medical Image Registration. in *2016 IEEE Conference on Computer Vision and Pattern Recognition Workshops (CVPRW)* 574–582 (2016). doi:10.1109/CVPRW.2016.78.
 39. van der Walt, S. *et al.* scikit-image: image processing in Python. *PeerJ* **2**, e453 (2014).
 40. Virtanen, P. *et al.* SciPy 1.0: fundamental algorithms for scientific computing in Python. *Nat. Methods* **17**, 261–272 (2020).

41. Desai, A. D. *et al.* DOSMA: A deep-learning, open-source framework for musculoskeletal MRI analysis. in *Proc. Intl. Soc. Mag. Reson. Med.* 27 (2019) (2019).
42. Pavlidis, T. Contour Filling. in *Algorithms for Graphics and Image Processing* 167–193 (Springer Berlin Heidelberg, 1982). doi:10.1007/978-3-642-93208-3_8.
43. Merkel, D. Docker: lightweight linux containers for consistent development and deployment. *Linux J.* **2014**, 2 (2014).
44. Ramírez, S. tiangolo/fastapi. <https://github.com/tiangolo/fastapi> (2023).
45. McKerns, M. M., Strand, L., Sullivan, T., Fang, A. & Aivazis, M. A. G. Building a Framework for Predictive Science. Preprint at <https://doi.org/10.48550/arXiv.1202.1056> (2012).
46. He, K., Zhang, X., Ren, S. & Sun, J. Deep Residual Learning for Image Recognition. in *2016 IEEE Conference on Computer Vision and Pattern Recognition (CVPR)* 770–778 (2016). doi:10.1109/CVPR.2016.90.
47. McRae, K. Catastrophic Interference is Eliminated in Pretrained Networks. (1993).
48. Martín Abadi *et al.* TensorFlow: Large-Scale Machine Learning on Heterogeneous Systems. (2015).
49. Chollet, F. & others. Keras. <https://keras.io> (2015).
50. Kingma, D. P. & Ba, J. Adam: A Method for Stochastic Optimization. Preprint at <https://doi.org/10.48550/arXiv.1412.6980> (2017).
51. Seabold, S. & Perktold, J. statsmodels: Econometric and statistical modeling with python. in *9th Python in Science Conference* (2010).